Thermal Event Recognition Applied to Protection of Tokamak Plasma Facing Components

Vincent Martin, Jean-Marcel Travere, Victor Moncada, François Brémond, and Gwenaël Dunand

***Abstract*—Magnetic confinement fusion tokamaks are complex devices where a large amount of power is required to make the fusion reactions happen. In such experimental conditions, Plasma Facing Components (PFC) are subjected to high heat fluxes which can damage them. Machine protection functions must then be developed to operate current and future devices like ITER in the safest way. In current tokamaks like Tore Supra, infrared thermographic diagnostics based on image analysis and feedback control are used to measure and monitor the heating of the PFC during plasma operation. The system consists in detecting high increase of the IR luminance signal beyond fixed qualitative levels for a set of predefined Regions of Interest (ROI). The detection of overheating regions is then fully dependent on the settings of the ROI and of the qualitative thresholds. This ROI-based approach must be improved to fit with ITER requirements and operation where the infrared scene complexity (many components monitored at the same time) will be a real challenge for the real-time PFC protection. In this paper, we propose a new vision-based approach for the automatic recognition of thermal events. This ROI-free approach, relying on intelligent vision system concepts, is composed of two main tasks: hot spot detection, and thermal event recognition. We present results of our approach for the recognition of one critical thermal event and compare its performance with the previous system.**

***Index Terms*—Infrared imaging diagnostics, tokamak, fusion plasma, machine protection, ITER, image and video processing, intelligent vision system**

I. Introduction

MAGNETIC confinement fusion is a more and more active field of research since nuclear fusion is considered as a promising approach for alternative energy production. One issue to reach a sufficient power balance in future devices like ITER is to rely on hot and long plasma produced and heated to thermonuclear temperatures by injecting large amounts of heating power (several MW or tens of MW). The goal is to inject most of the available power while ensuring the Plasma Facing Components (PFC) safety by limiting the power load just below their operational limits. In the long pulse experiments of Tore Supra, and in contrast with short pulse experiments, the plasma facing components must be actively cooled down by a fast water flow, close to the plasma surface, in order to maintain their temperature sufficiently low to avoid melting and/or impurity pollution of the plasma (a unique feature of Tore Supra among other tokamaks). Any failure can lead to a water leak and time consuming repairs. To measure and monitor the heating of the PFC during plasma operation, the most efficient way is to collect true surface temperature information using a network of infrared video cameras. This is why Tore Supra, which is a carboneous device (emissivity $\sim$ 1), is equipped with a comprehensive infrared viewing system [1] made of seven endoscopes bodies equipped so far with eight infrared cameras (see figure 1). In the same way, the current ITER optical design [2] envisages a network of twelve infrared cameras distributed in four equatorial port-plugs, covering up to 70% of the vacuum chamber.

The infrared camera array of Tore Supra is routinely used as input of a feedback control system based on early detecting local hot spots to control in real-time the heating power sources. More details on this unique operational control system can be found in [3].

[Fig. 1 about here.]

The image analysis part of the Tore Supra feedback control consists in detecting high increase of the IR luminance signal beyond fixed qualitative levels for a set of predefined Regions of Interest (ROI) (see figure 2). The ROI are defined according to the geometry of monitored objects (e.g. copper mouth, lateral protection, etc.). It has been successfully applied to the detection of some thermal events [4], as electrical arcing discussed here.

[Fig. 2 about here.]

Due to increase of data volumes and scene complexity, this ROI-based approach must be improved to fit with ITER requirements and operation, as stated in [4]. Indeed, this system has several drawbacks and limitations listed below:

1) working with true surface temperature values makes the strong assumption that the infrared digital sensors are always well calibrated and the optical transmission factors as well as optical properties of observed materials (e.g. emissivity) are well-known,
2) it requires an operator for: (1) editing the ROI each time the PFC configuration changes or when the camera field of view has been modified after a discharge, and (2) tuning of the qualitative thresholds (time-consuming tasks),
3) thermal events that occurs outside of the ROI cannot be detected,
4) the sensitivity to false detection is high: the presence of only one noisy or dead pixel in a ROI with a infrared

V. Martin and F. Brémond are with the Pulsar project-team, INRIA Sophia Antipolis Méditerranée, 2004 route des Lucioles BP 93, F-06902 Sophia Antipolis cedex, France. Phone: (+33)492387659, email: {vrmartin,fbremond}@sophia.inria.fr

J.M. Travere and V. Moncada are with CEA, IRFM, F-13108 Saint Paul-lez-Durance, France. Phone: +33442256367 Email: {jean-marcel.travere,victor.moncada}@cea.fr

G. Dunand is with Sophia Conseil Society, Research & Engineering Department, F-06560 Sophia Antipolis, France. Phone: +33442256367 Email: gwenael.dunand@cea.fr

luminance higher than the qualitative detection threshold is enough to raise a false alarm,
5) different thermal events will not be discriminated if they occur in the same ROI,
6) Extrapolated to wide-angle view systems as planned for ITER, manual drawing of ROI should be extremely difficult to operate routinely.

In summary, a need exists in both improvement of the infrared video processing and better understanding and interpretation of infrared images as, for instance, an accurate identification of new heating zones (hot spots). In this paper, we propose a new approach for the automatic detection of Thermal Events (TE) inspired from a video understanding framework [5] widely used in video surveillance applications.

The major advantages of such a framework compared to the current system and its previously listed issues can be justified as follows:

- this is a qualitative image analysis approach as described in [6], relying on spatio-temporal pattern matching techniques. The knowledge of precise optical properties of monitored object (e.g. emissivity of metal) is then minimized.
- this is a ROI-free approach: the *a priori* knowledge of a TE is not inside the image but in the TE description model used to specialize generic image processing operators.

The paper is organized as follows: we first detail in section II the different steps of the proposed approach for the automatic detection and recognition of thermal events in infrared videos. As a first step to validate this new approach, we focus on arcing event recognition in section III. Section IV reports the recognition results on experimental data with a quantitative performance evaluation and comparison with the current system used at Tore Supra. Finally, conclusions as well as future perspectives are discussed in section V.

II. Thermal events recognition

The goal of our video understanding framework is to separate the expert knowledge of event modeling from the image processing tasks dedicated to the extraction of low level features from visual data. To this end, we follow a bottom-up approach (from pixel to semantic interpretation) illustrated in figure 3 where each of the two main vision tasks (i.e. hot spot detection and thermal event recognition) is specialized (e.g. parameter tuning) thanks to the formalized description of observed TE. At the first stage (hot spot detection), we just identify localized hot spots but still not characterize them. A reasoning process is then necessary to recognize the thermal phenomena called Thermal Events (TE).

[Fig. 3 about here.]

A. a priori knowledge of thermal events

The interpretation of observed hot spots mostly relies on *a posteriori* physical analysis. The goal is to explain the origin of these hot spots by the study of their temporal evolution and their localization. Some representatives TE identified during a plasma discharge are shown in figure 4 and correspond to:

- Local **RF sheath effect**: localized on the top left corner of the Faraday screen (made of stainless steel with B_4C coating), this hot spot is suspected to be due to local RF electrical field carrying an enhanced power onto the antenna as explained in [7]. The deposited power causes hot spots with risk of melting and bursts of metallic impurities.
- **Accelerated electrons** from lower hybrid: localized on the left side protection (made of graphite tiles), this hot spot is suspected to be due to electrons accelerated in the near field of the lower hybrid launcher which is magnetically connected to the ICRH antenna as explained in [8].
- **Fast ion losses**: localized both on the side protection and the vertical edge of the Faraday screen, it might be caused by fast ions losses created during ICRH hydrogen minority heating scheme as explained in [9]. In Tore Supra, these losses are an important cause of concern for the long pulse capability at high RF power levels due to high magnetic ripple (see [10]).
- B_4C **flakes**: the hot spot has a small size and is localized on the vertical edge of the Faraday screen. It is due to the flaking of the B_4C coating consequently to the heating caused by fast ion losses as shown in [11]. Infrared luminance may overpass the acceptable threshold without apparent risk of damage.
- **Electrical arcs**: they are caused by a potential difference between the two lateral shields of a heating antenna during high power discharges, and can lead to the destruction of sensitive parts like the copper mouth of the antenna.
- specular/diffuse **reflection** area of the limiter on metallic component (see [12]) that may induce false detection.

[Fig. 4 about here.]

B. a priori knowledge formalization

We use a formalized visual description of the thermal events to detect as a support of reasoning mechanisms. This description relies on a visual concept ontology composed of generic spatio-temporal attributes such as geometric and temporal cues introduced in [13]. The main advantage in using such a symbolic description is its re-usability in different experimental contexts. For instance, the description of a TE does not change if the image acquisition system is modified. Indeed, visual concepts are an intermediate level that helps mapping low-level numerical values to a domain class description. We detail in figure 5 the TE class hierarchy that should be considered as an extendable basis. This hierarchy as well as the knowledge associated with each class have been defined with physicists.

[Fig. 5 about here.]

III. Automatic arcing event recognition

A. Arcing event knowledge formalization

For the specific case of electrical arcing, physicists describe them through their shape and their specific infrared luminance

dynamic. Arc shape and luminance ranges are two discriminative characteristics that can be mapped into low level features to be extracted from visual data. Corresponding knowledge representation in terms of spatio-temporal attributes is given in Figure 6. Range values associated with each attributes have been manually learnt on a set of representative TE samples.

[Fig. 6 about here.]

The visual attributes have been chosen for their low computational cost. The local contrast of a region r is defined as the ratio $\frac{|\mu_r - \mu_{nr}|}{(\mu_r + \mu_{nr})}$ where μ_r is the mean value of the pixels in region r and μ_{nr} the mean value of the pixels surrounding the region r. The L gradient is the positive variation of the infrared luminance $\Delta L = L_i - L_{i-1}$ between the time interval $\Delta t = t_i - t_{i-1}$.

B. Transient hot spot detection

Motion is a particularly important cue for object detection in image sequences. Indeed, a moving object is often referred as an object of interest and can then be classified as foreground. The simplest approach to detect moving pixel in image sequences consist in subtracting the current frame from a reference frame. Since background is rarely stationary, the key issue for any background subtraction algorithm is to efficiently model the background and update it according to the pixel variations. Many approaches have been proposed to background modeling based on unimodal distribution, mixture of gaussians or compressed models (see [14] for an overview). Here the method of Butler et al. [15] is used. This algorithm has a low computational cost and is adapted to multi-modal backgrounds. The basic idea of this method is to maintain some limited but important information about the history of each pixel. To this end, the algorithm models each pixel in the frame by a group of *clusters* where each cluster consists of an average pixel value called the *centroid* with an associated *weight* representing the cluster proportion among the others. The clusters are sorted in order of the likelihood that they model the background and their weighs and centroids are adapted to deal with background changes. An incoming pixel is then classified into background/foreground pixel with regards to the weight of the matched cluster. The algorithm depends on three main free parameters: the number of clusters, the adaptation rate, and the foreground classification threshold. The adaptation rate is directly linked up to the thermal evolution of the thermal event to detect. A small rate will be adapted to the detection of slow thermal events whereas a high rate will be adapted to the detection of transient thermal events such as electrical arcing. Therefore the setting of this parameter depends directly on the *a priori* knowledge given by the experts. In the same way, the foreground classification threshold can be connected to the infrared luminance attributes. Basically, the parameter is set according to the local contrast attribute of the thermal event. In the case of arcing events, we estimated this parameter according to the average contrast value computed from a set of identified arcing events. Concerning the number of clusters, we observed only small detection differences while varying the value (between 2 and 5), so we decided to set it to three in order to maintain a good trade-off between sensitivity and frame rate.

C. Arc pattern reconstruction

Electrical arcs are oriented horizontally (in the video camera referential) with a strong infrared signature at the copper mouth level. Nevertheless, it is very rare to observe the entire pattern in the infrared images. Most of the time, only a collection of pattern subparts are visible and detected in the form of several blobs by the segmentation algorithm. This is why a specific merging process is necessary to reconstruct the whole arcing pattern.

[Fig. 7 about here.]

According to the symbols used in figure 7, we have defined a blob merging criterion C as follows:

$$C = c_1 \wedge c_2 \quad (1)$$

where, $\forall\ i, j = 1, 2,\ i \neq j$

$$c_1 = \{|y_{O_i} - y_{O_j}| < |y_{I_i} - y_{O_j}|\} \quad (2)$$

$$c_2 = \{w_1 + w_2 < \frac{1}{2} \times |x_{O_i} - x_{O_j}|\} \quad (3)$$

This criterion favors the merge of blobs having the same orientation (here horizontal for the arcs) and capable of *seeing* each other in this orientation. Two blobs B_1 and B_2 are defined as visible for each other if the center of B_1 (resp. B_2) is inside the hatched zone formed by B_2 (resp. B_1) as seen in figure 7. The visibility is proportional to the inverse of the distance, to the sizes, and to the horizontal elongations of the two blobs (parameters d, w, and h). This criterion prevents from merging distant small blobs. Then, a new bounding box including the two merged blobs is computed and the merging process is repeated until no more merges are possible.

D. Arcing event recognition

Once each blob has been filtered/merged, the next task is to look for evidence of given described events from the detected transient hot spots. To this end, we also rely on the *a priori* knowledge of figure 6. In a deep-first search procedure, each hypothesis leading to the recognition of a TE is tested. The goal is to traverse the domain class hierarchy from the most abstract class (top of the tree) to the targeted TE. If the test fails at one specific layer, the recognition procedure stops at the previous layer. For the specific case of arcing event (third layer of our TE class hierarchy), we use three criteria for the event recognition:

1) pattern duration (transient event layer)
2) pattern shape (electrical arcing layer)
3) pattern size (electrical arcing layer)

The recognition algorithm verifies that all attribute values extracted from the merged blobs are within the corresponding learned values. We observe that geometric attributes prevail, most of the time, upon the other attributes (i.e. infrared luminance and temporal attributes) for the arcing event recognition. In the same way, the discrimination between arc and residual

arc (i.e. arcs lasting more than 300 milliseconds) is based on arc pattern duration. To this end, arc patterns must be tracked as explained in the next section.

E. Arcing event tracking

If a new electrical arcing pattern is recognized, an identifier is associated with the corresponding bounding box and 2D coordinates of the pattern is stored in a buffer. Then, at each frame, newly detected arc patterns are matched with the ones present in the buffer. The matching criterion is based on a minimal vertical distance between the two centers of the pattern matching candidates (here set at 10 pixels). Indeed, we have observed that arc patterns often occur at specific levels related to the geometry of the antenna mouth. Each of these levels has a height of 20 pixels approximatively so a distance criterion of 10 pixels prevents from merging arc patterns located at two different levels. Once an arc pattern has been recognized, we trigger the background model updating of the detected pixels in the corresponding bounding box so that a possibly residual arc pattern is not integrated into the background model (cases of missed detection in [16]). The trigger action consists in setting two parameters of the background model update algorithm, namely the learning rate and the matching threshold parameters, to lower values. The parameters are automatically set to initial values when the arc pattern disappears.

IV. Recognition Results

A. Performance Evaluation of the proposed approach

To assess the performance of our approach, we have compared the results of the arcing event recognition with validation data obtained from manual annotations of a pulse dataset. The pulse dataset used for this evaluation is composed of 50 infrared films of two heating antenna views, corresponding to a total plasma time of 1496 seconds with a discharge duration between 5 and 62 seconds. The pulses have been chosen over the overall database so as to represent all plasma scenarios for which arcs are used to be observed. Only 9 pulses do not contain any arcing events. A total of 197 arcing events have been annotated by three human subjects trained to recognize arcing events in infrared videos. Figure 8 presents qualitative results for three representative cases.

[Fig. 8 about here.]

Counting results are reported in table I. A true positive corresponds to a detected arc present in the annotation base. A false negative corresponds to an arc not detected but present in the annotation base. A false positive corresponds to a detected arc not present in the annotation base.

[TABLE 1 about here.]

We have identified two sources of explanation for the false negative results:

1) The annotation is sometime ambiguous when arcs are very close in time or when the infrared signal is not sufficiently clear enough to visually identify an arcing event.
2) Most of the false negative results corresponds to borderline cases, i.e. when the arcs are very thin and/or weak. In this case, the pattern reconstruction algorithm often fails in merging the blobs (see figure 9). One improvement should be the triggering of the foreground classification parameter by the injected power signal, since weak arcs occur during low power discharges only.

False positive cases during plasma current ramp-up mentioned in [16] have been resolved thanks to the trigger of detection and recognition algorithms by the injected power signal.

[Fig. 9 about here.]

Figure 10 presents an example of a residual arc recognition.

[Fig. 10 about here.]

B. Performance comparison with the arc detection algorithm used at Tore Supra

The algorithm used at Tore Supra for arcing event detection is based on a weighted running average over two successive frames (at time noted t and $t-1$), on the maximum infrared luminance (noted ΔL) extracted from the union of two ROI defined for electrical arcing (see Figure 2). The computation of the infrared luminance threshold τ is triggered by the injected power noted P_{inj}. The output is a binary signal noted S_{ARC} such as:

$$S_{ARC}(t) = (\Delta L(t) > \tau(t)) \ \wedge \ (I_p(t) > 0.1) \tag{4}$$

where I_p is the plasma current, and

$$\Delta L(t) = L(t) - \frac{3 \times L(t-1) + L(t)}{4} \tag{5}$$

$$\Delta P_{inj}(t) = P_{inj}(t) - \frac{3 \times P_{inj}(t-1) + P_{inj}(t)}{4} \tag{6}$$

$$\tau(t) = \alpha(1 + \alpha \Delta P_{inj}(t)) \tag{7}$$

$$\text{with } \alpha = 30 \tag{8}$$

Table II summarizes the detection results of this algorithm together with the results of the proposed approach. Since S_{ARC} is not available for all pulses of the data set used in Table I, the test dataset has been reduced to 18 infrared films where 90 arcing events have been annotated, still representing a good sampling of the different scenarios.

[TABLE 2 about here.]

Our proposed approach outperforms the current arc detection algorithm especially in terms of false detections. This large difference makes evidence of the brittleness of the thresholding technique of the current system. The practical consequence of using the proposed approach for real-time control of the launched power would be a better optimization of the power injection.

C. Computational performance

In the perspective of a real-time implementation, we have assessed the computation speed of the proposed approach. The infrared videos are acquired at 50 frames per seconds.

The image size is 320×240 pixels. The frame rate of the C++ software implementation on 2×2.33GHz PC is about 20 frames per second. As seen in Table III, the most important part of the computational time is taken by the detection algorithm. This results is obviously coherent since at this stage, the amount of information to proceed is equal to the number of pixels. Recognition and tracking algorithms have much less memory and CPU needs since they just manipulate a list of bounding box coded on only four values (upper left and bottom right positions of the box). With an FPGA implementation of the detection algorithm, the processing should be able to deliver results every 20 milliseconds, i.e. at the camera frame rate.

[TABLE 3 about here.]

V. Conclusion and future work

In this paper, we have proposed a new vision-based approach for the automatic recognition of thermal events in infrared images of PFC. The proposed approach improves the current PFC monitoring system used at Tore Supra and addressing arcing event recognition. As a result, the false detection rate is drastically reduced. As a consequence for real time control, the power injection should be better optimized. Moreover, this ROI-free approach is independent of any displacement inside the camera field of view with a better localization of the observed thermal events. This approach is going to be extended to the recognition of other thermal events (e.g., B_4C flakes, accelerated electrons, fast particle losses, etc.) to prove its genericity. A three dimensional scene model will be added to take into account, at each step of the thermal event recognition process, the geometrical description of the monitored objects and their optical properties. The ultimate goal of this project is to improve the reliability of the current real-time control acting on the heating sources. To this end, the hot spot detection algorithm will be implemented on a FPGA to reach real-time constraints, and the system will be tested during Tore Supra plasma operation. This will be a good starting point toward a real-time automatic feedback control system based on intelligent signal and image processing applied to the foreseen infrared wide angle viewing system of ITER which will be involved in the crucial PFC protection function.

Acknowledgment

This work, supported by the European Communities under the contract of Association between EURATOM and CEA, was carried out within the framework of the European Fusion Development Agreement. The views and opinions expressed herein do not necessarily reflect those of the European Commission.

The authors would like to acknowledge the reviewers for their substantial comments.

References

[1] D. Guilhem et al., "Tore-supra infrared thermography system, a real steady-state diagnostic," *Fusion Engineering and Design*, vol. 74, no. 1-4, pp. 879 – 883, 2005, Proceedings of the 23rd Symposium of Fusion Technology.

[2] S. Salasca et al., "Development of equatorial visible/infrared wide angle viewing system and radial neutron camera for iter," *Fusion Engineering and Design*, vol. 84, no. 7-11, pp. 1689 – 1696, 2009, Proceeding of the 25th Symposium on Fusion Technology.

[3] Ph. Moreau et al., "Rf heating optimization on tore supra using feedback control of infrared measurements," *Fusion Engineering and Design*, vol. 82, no. 5-14, pp. 1030 – 1035, 2007, Proceedings of the 24th Symposium on Fusion Technology.

[4] J.-M. Travere and Tore Supra team, "In-vessel components imaging systems: From the present experience towards iter safe operation," *Fusion Engineering and Design*, vol. 84, no. 7-11, pp. 1862 – 1866, 2009.

[5] F. Brémond, M. Thonnat, and M. Zuniga, "Video understanding framework for automatic behavior recognition," *Journal on Behavior Research Methods*, vol. 3, no. 38, pp. 416–426, 2006.

[6] R. Reichle et al., "On the operational specifications and associated R&D for the VIS/IR diagnostic for ITER," in *Int. Conf. on Advancements in Nuclear Instrumentation, Measurement Methods and their Applications*, June 2009.

[7] L. Colas et al., "Hot spot phenomena on Tore Supra ICRF antennas investigated by optical diagnostics," *Nuclear Fusion*, vol. 43, pp. 1–15, Jan. 2003.

[8] M. Goniche et al., "Enhanced heat flux in the scrape-off layer due to electrons accelerated in the near field of lower hybrid grills," *Nuclear Fusion*, vol. 38, no. 6, pp. 919–937, 1998.

[9] V. Basiuk et al., "Ripple losses during icrf heating in tore supra," *Nuclear Fusion*, vol. 44, no. 1, pp. 181–192, 2004.

[10] A. Ekedahl et al., "Operational limits during high power long pulses with radiofrequency heating in tore supra," *Nuclear Fusion*, vol. 49, no. 9, pp. 095010, 2009.

[11] M. Chatelier *on behalf of* Equipe Tore Supra, "Integration of high power, long pulse operation in tore supra in preparation for iter," *Nuclear Fusion*, vol. 47, no. 10, pp. S579–S589, 2007.

[12] D. Guilhem, R. Reichle, and H. Roche, "Reflections and surface temperature measurements in experimental fusion reactors tore-supra, jet and iter," *Quantitative InfraRed Thermography Journal*, vol. 3, no. 2, pp. 155–168, 2006.

[13] N. Maillot and M. Thonnat, "Ontology based complex object recognition," *Image Vision Comput.*, vol. 26, no. 1, pp. 102–113, 2008.

[14] R.J. Radke, S. Andra, O. Al-Kofahi, and B. Roysam, "Image change detection algorithms: a systematic survey," *IEEE Transactions on Image Processing,*, vol. 14, no. 3, pp. 294–307, March 2005.

[15] Darren E. Butler, Jr. V. Michael Bove, and Sridha Sridharan, "Real-time adaptive foreground/background segmentation," *EURASIP J. Appl. Signal Process.*, vol. 2005, no. 1, pp. 2292–2304, 2005.

[16] V. Martin, J.-M. Brémond, F. Travere, V. Moncada, and G. Dunand, "Thermal event recognition applied to tokamak protection during plasma operation," in *IEEE International Instrumentation and Measurement Technology Conference*, May 2009, pp. 1690–1694.

LIST OF FIGURES

1 Overview of one of the seven endoscopes used to monitor PFC as heating antennas. 7
2 ROI drawn by the user (in white) for the monitoring and the feedback control to prevent from PFC overheating. Qualitative thresholds on infrared luminance signal are indicated for each ROI. 8
3 Process chain of the proposed approach. The algorithm is first triggered by the value of the injected power P_{inj} through a fixed threshold T_P (here fixed at 0.1MW) to avoid, for instance false detection of arcing event during plasma current ramp-up. 9
4 Time-traces of some identified hot spots (picked from the infrared frames) and of the power injection (bottom plots) during a plasma discharge for two heating antennas. 10
5 Domain class hierarchy representing the different abstraction layers used to characterize the different Thermal Events (TE). Associated knowledge representation of TE in bold face is described in Figure 6 11
6 High-level description of `arc` and `residual arc` events through the different abstraction layers defined in Figure 5. For simplification purposes, spatial attributes have been translated from physical dimensions to pixel values, and temporal attributes have been translated from seconds to frames. Ranges values corresponds to observed min and max. 12
7 Blobs features (w, h, o) and inter-blob features (d, I) used by the merging criteria. 13
8 Ground truth with corresponding bounding box superimposed on original images (top), process outputs after transient change detection, detected pixels are in black (row 1), median filtering and blob extraction (row 2), pattern reconstruction (row 3), and arcing event detection with corresponding bounding box superimposed on original images (bottom). 14
9 One example of typical missed detection. This is a borderline case when arc is very weak (low power injection). Despite the quite good detection, the algorithm fails to reconstruct the arc pattern due to too small and unfavorably oriented blobs. 15
10 Residual arc event (i.e. arc lasting more than 300 ms) detected by our approach (right) after successful tracking of the same arc pattern #0 (left) during 740 ms. 16

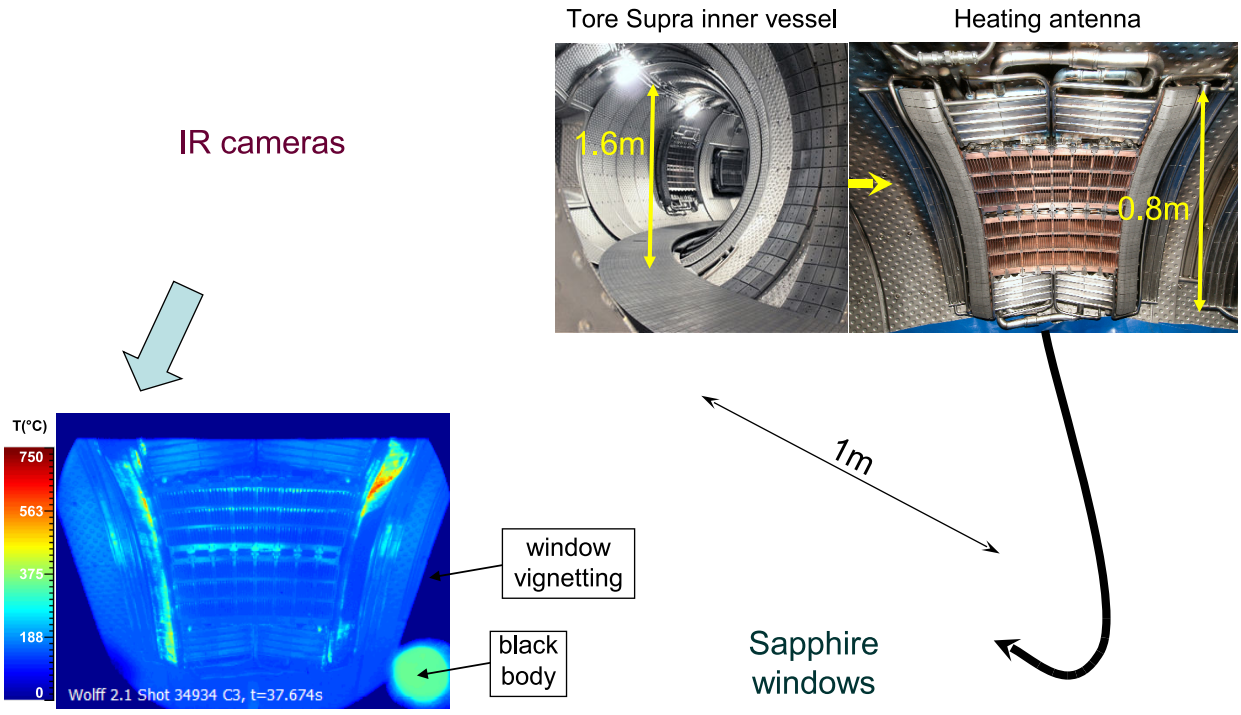

Fig. 1. Overview of one of the seven endoscopes used to monitor PFC as heating antennas.

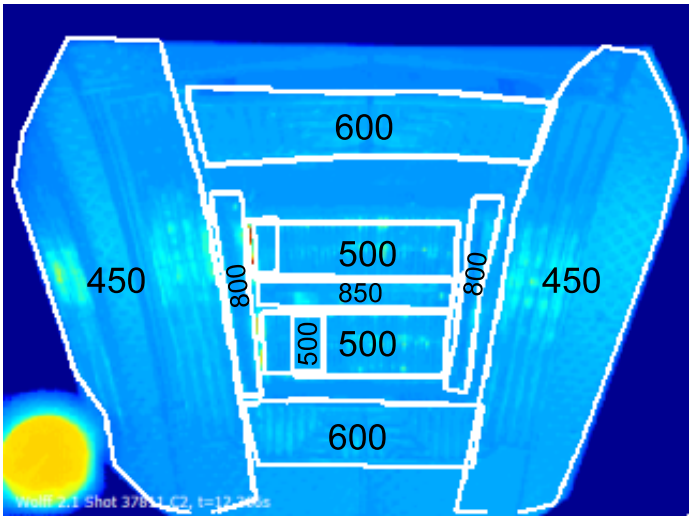

Fig. 2. ROI drawn by the user (in white) for the monitoring and the feedback control to prevent from PFC overheating. Qualitative thresholds on infrared luminance signal are indicated for each ROI.

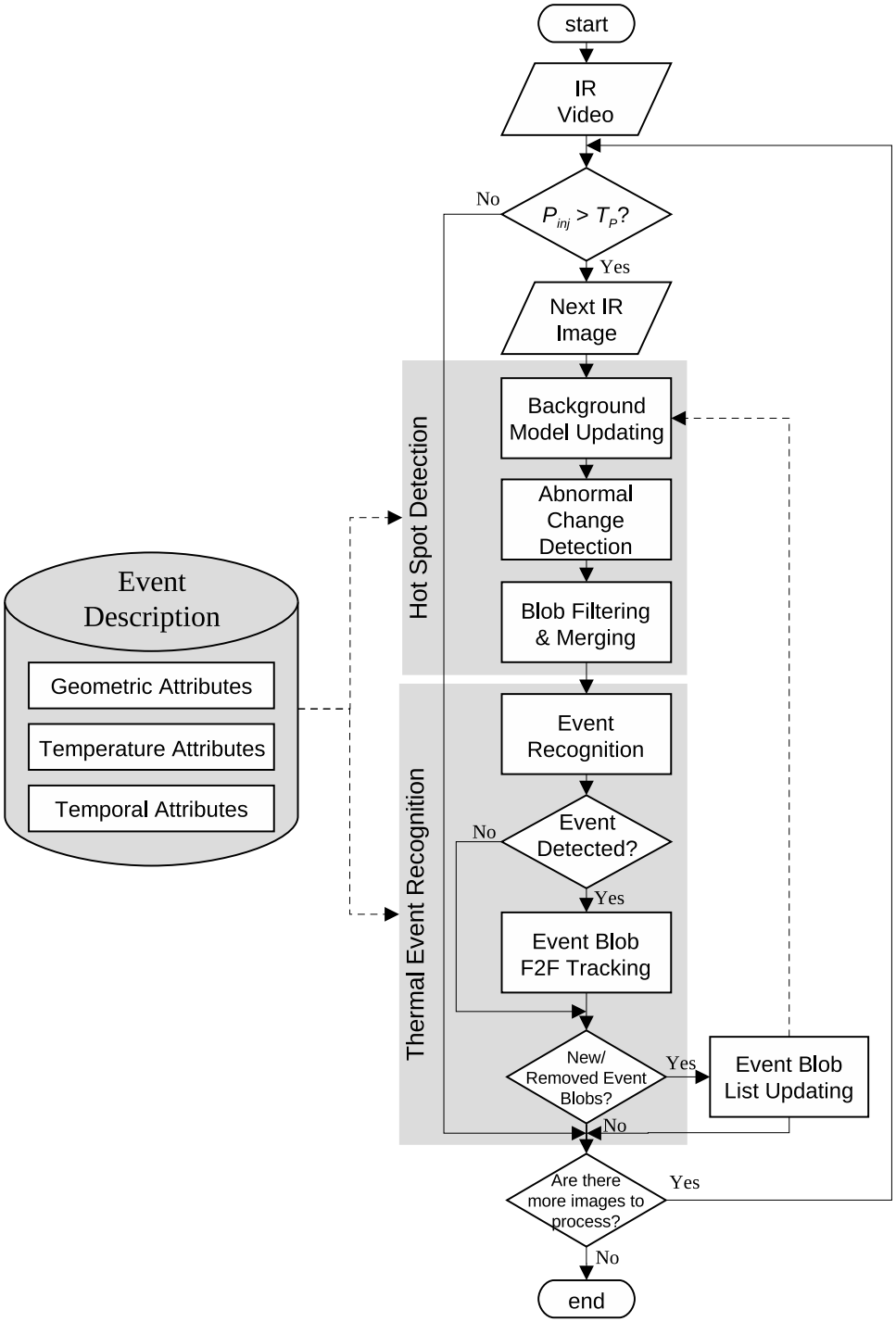

Fig. 3. Process chain of the proposed approach. The algorithm is first triggered by the value of the injected power P_{inj} through a fixed threshold T_P (here fixed at 0.1MW) to avoid, for instance false detection of arcing event during plasma current ramp-up.

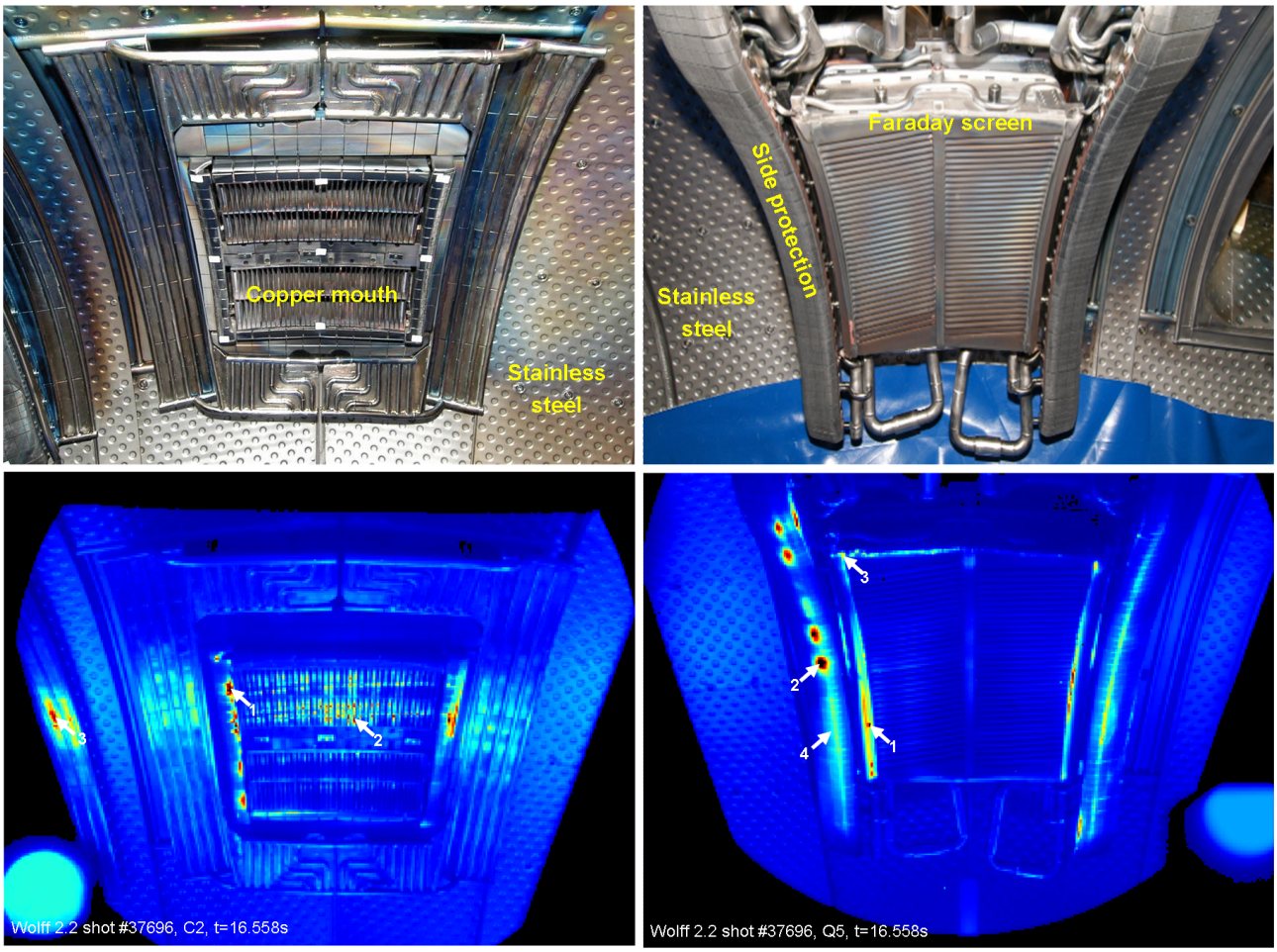

(a) Identified hot spots on two heating antennas. Left column: the lower hybrid current drive (LHCD), and right column: the ion cyclotron resonance heating antenna (ICRH).

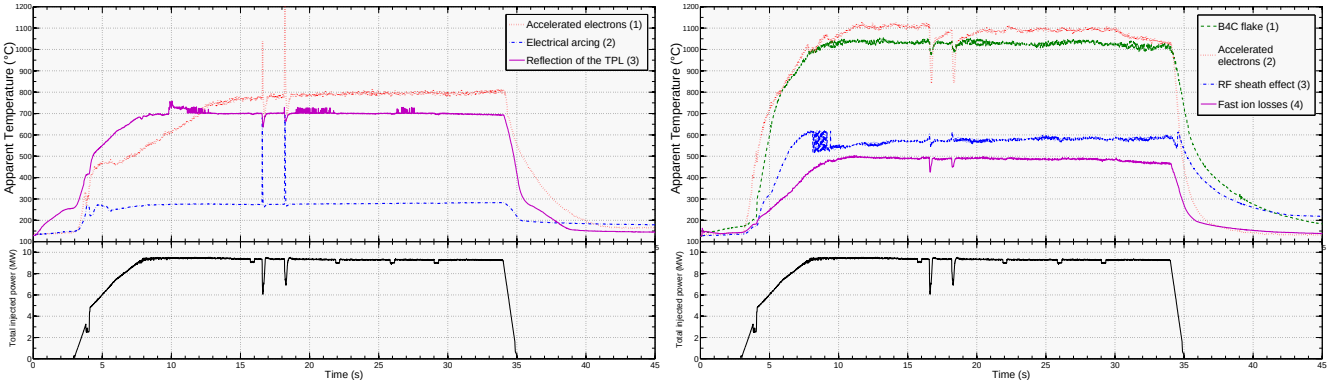

(b) Time-traces of the apparent temperature of the picked pixels in (a) (left: LHCD hot spots, right: ICRH hot spots)

Fig. 4. Time-traces of some identified hot spots (picked from the infrared frames) and of the power injection (bottom plots) during a plasma discharge for two heating antennas.

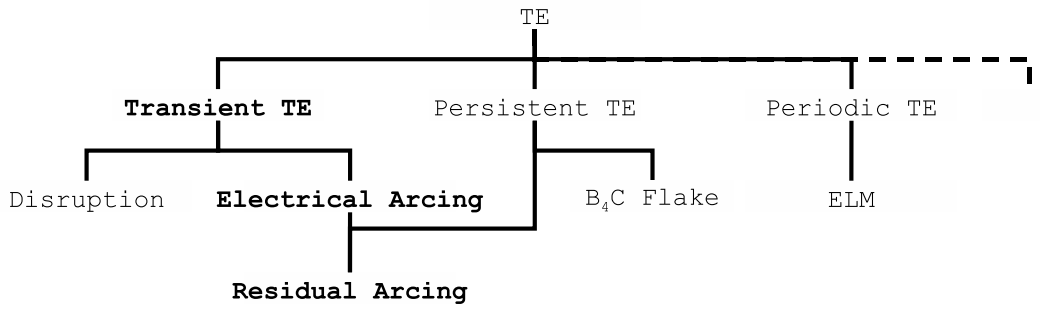

Fig. 5. Domain class hierarchy representing the different abstraction layers used to characterize the different Thermal Events (TE). Associated knowledge representation of TE in bold face is described in Figure 6 .

Domain Class Transient Event **SuperClass** Thermal Event
Temporal Attributes

Duration	[1	8]
L gradient	[154	347]

Domain Class Electrical Arcing **SuperClass** Transient Event
Spatial Attributes

Length	[50	110]
Height	[7	20]
Elongation	[2.5	16]
Area	[120	2200]

Infrared Luminance Attributes

Local contrast	[1.3e-4	0.17]
Entropy	[3.8	9.02]

Domain Class Residual Arcing **SuperClass** Electrical Arcing **and** Residual TE

Domain Class Residual TE **SuperClass** Thermal Event
Temporal Attributes

Duration	[15	Inf]

Fig. 6. High-level description of `arc` and `residual arc` events through the different abstraction layers defined in Figure 5. For simplification purposes, spatial attributes have been translated from physical dimensions to pixel values, and temporal attributes have been translated from seconds to frames. Ranges values corresponds to observed min and max.

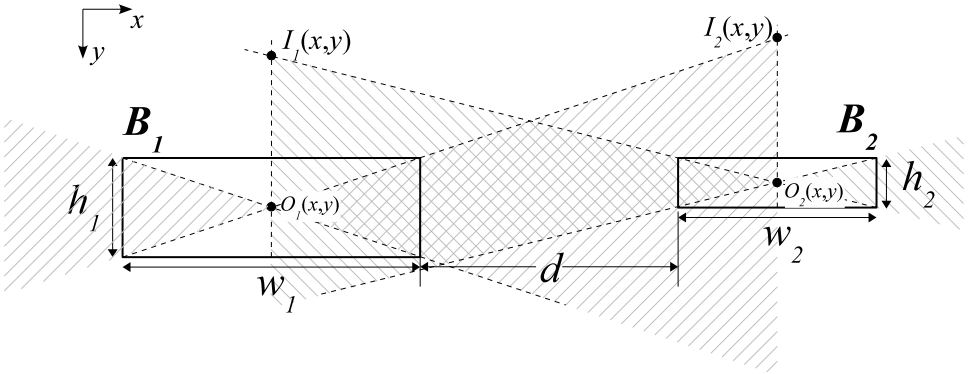

Fig. 7. Blobs features (w, h, o) and inter-blob features (d, I) used by the merging criteria.

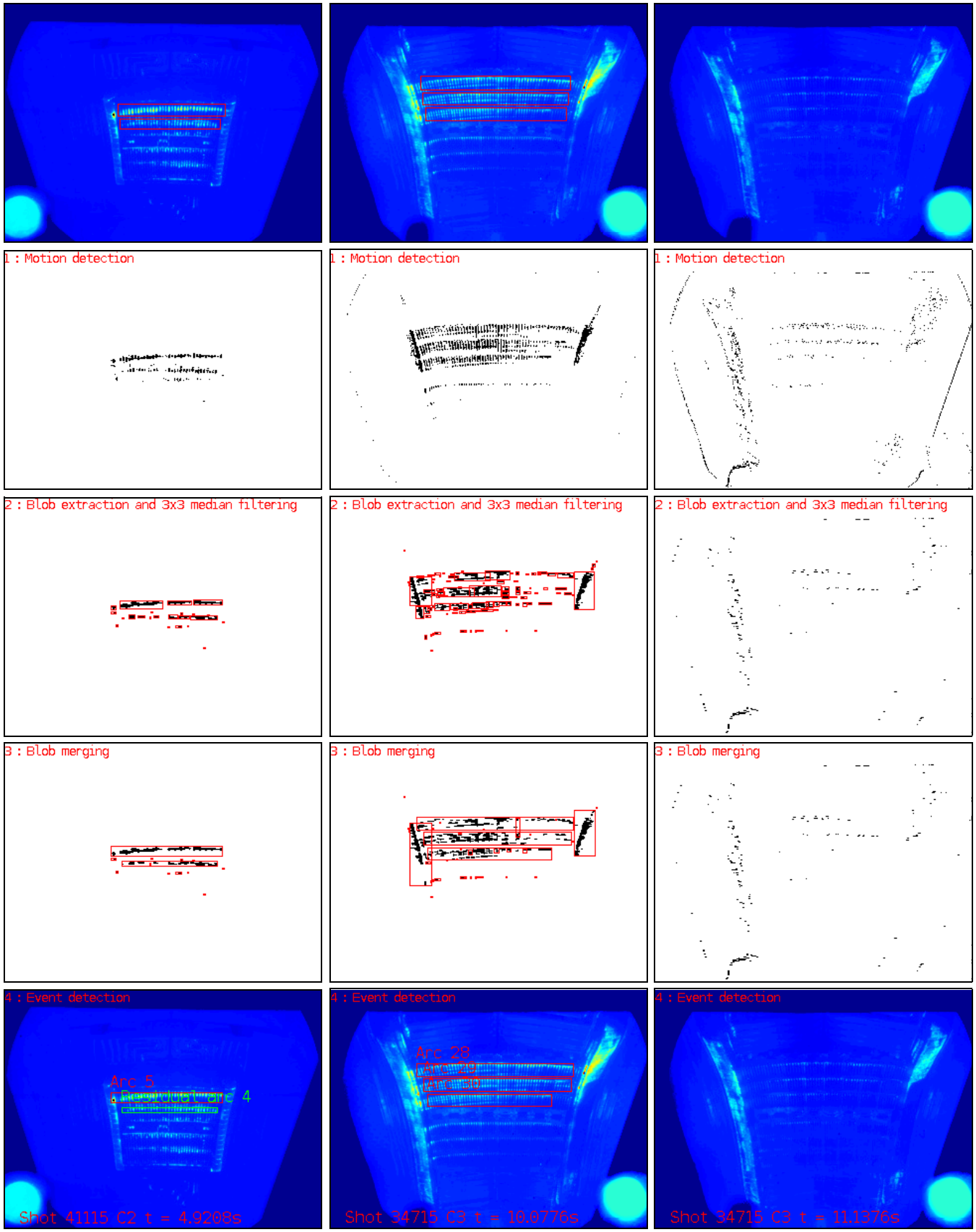

Fig. 8. Ground truth with corresponding bounding box superimposed on original images (top), process outputs after transient change detection, detected pixels are in black (row 1), median filtering and blob extraction (row 2), pattern reconstruction (row 3), and arcing event detection with corresponding bounding box superimposed on original images (bottom).

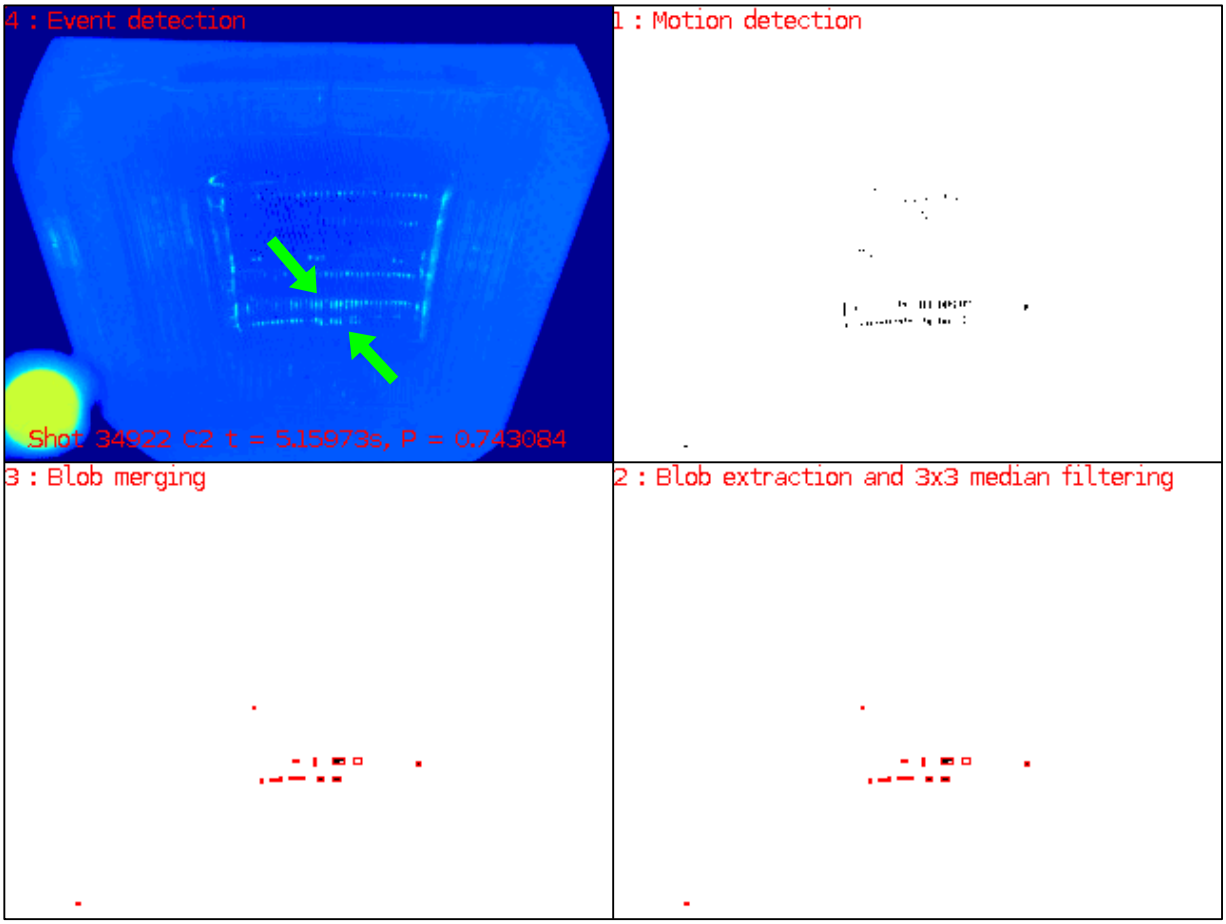

Fig. 9. One example of typical missed detection. This is a borderline case when arc is very weak (low power injection). Despite the quite good detection, the algorithm fails to reconstruct the arc pattern due to too small and unfavorably oriented blobs.

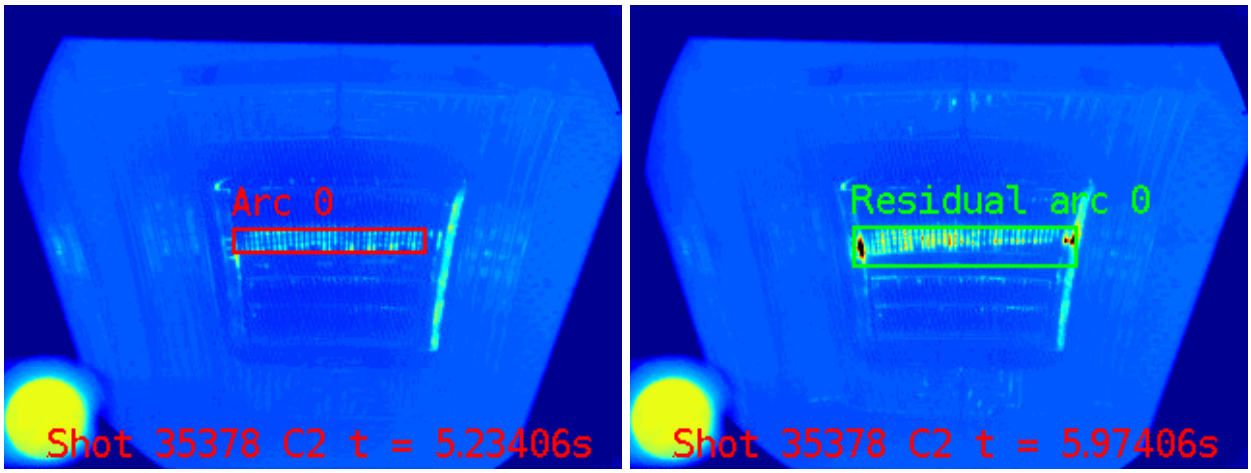

Fig. 10. Residual arc event (i.e. arc lasting more than 300 ms) detected by our approach (right) after successful tracking of the same arc pattern #0 (left) during 740 ms.

LIST OF TABLES

I Arcing event recognition results obtained with the proposed approach with corresponding ground truth (GT), true positive (TP), false negative (FN), and false positive (FP) counts. 18
II Comparison between the arcing event detection results obtained with the current system used at Tore Supra and with the proposed approach in bold face. 19
III Computation time for each step of the proposed approach. 20

Antenna	no. of pulses	Annotated arcing events	no. of detected arcing events with our approach		
			TP	FN	FP
C2	28	140	133	7	0
C3	22	57	49	8	2
C2 + C3	50	197	182	15	2

TABLE I

ARCING EVENT RECOGNITION RESULTS OBTAINED WITH THE PROPOSED APPROACH WITH CORRESPONDING GROUND TRUTH (GT), TRUE POSITIVE (TP), FALSE NEGATIVE (FN), AND FALSE POSITIVE (FP) COUNTS.

Antenna	no. of pulses	Annotated arcing events	no. of detected arcing events		
			TP	FN	FP
C2	11	73	68/**70**	5/**3**	51/**0**
C3	7	17	11/**13**	6/**4**	7/**0**
C2 + C3	18	90	79/**83**	11/**7**	58/**0**

TABLE II
COMPARISON BETWEEN THE ARCING EVENT DETECTION RESULTS OBTAINED WITH THE CURRENT SYSTEM USED AT TORE SUPRA AND WITH THE PROPOSED APPROACH IN BOLD FACE.

process	processing time (in ms)	% of the total frame rate
detection	41.0	80
recognition	3.3	7
tracking	6.7	13
overall	51.0	100

TABLE III
COMPUTATION TIME FOR EACH STEP OF THE PROPOSED APPROACH.